magnetochemistry

MDPI

Article

Evaluation of the Effect of Silica Fume on Amorphous Fly Ash Geopolymers Exposed to Elevated Temperature

Ong Huey Li [1,2], Liew Yun-Ming [1,2,*], Heah Cheng-Yong [1,2], Ridho Bayuaji [3], Mohd Mustafa Al Bakri Abdullah [1,2], Foo Kai Loong [4], Tan Soo Jin [1,2], Ng Hui Teng [1,2], Marcin Nabiałek [5], Bartlomiej Jeż [5] and Ng Yong Sing [1,2]

1 Geopolymer and Green Technology, Centre of Excellence (CEGeoGTech), Universiti Malaysia Perlis (UniMAP), Perlis 01000, Malaysia; hueyil_shiro@hotmail.com (O.H.L.); cyheah@unimap.edu.my (H.C.-Y.); mustafa_albakri@unimap.edu.my (M.M.A.B.A.); sjtan@unimap.edu.my (T.S.J.); venessa42@live.com (N.H.T.); nicholas.zai.1130@gmail.com (N.Y.S.)
2 Faculty of Chemical Engineering Technology, Universiti Malaysia Perlis (UniMAP), Perlis 01000, Malaysia
3 Department of Civil Infrastructure Engineering, Faculty of Vocations, Institut Teknologi Sepuluh Nopember, Surabaya 60111, Indonesia; bayuaji@ce.its.ac.id
4 Institute of Nano Electronic Engineering (INEE), Universiti Malaysia Perlis (UniMAP), Perlis 01000, Malaysia; klfoo@unimap.edu.my
5 Department of Physics, Faculty of Production Engineering and Materials Technology, Częstochowa University of Technology, Al. Armii Krajowej 19, 42-200 Częstochowa, Poland; nmarcell@wp.pl (M.N.); bartek199.91@o2.pl (B.J.)
* Correspondence: ymliew@unimap.edu.my

Abstract: The properties of amorphous geopolymer with silica fume addition after heat treatment was rarely reported in the geopolymer field. Geopolymer was prepared by mixing fly ash and alkali activator. The silica fume was added in 2% and 4% by weight. The geopolymer samples were cured at room temperature for 28 days before exposed to an elevated temperature up to 1000 °C. The incorporation of 2% silica fume did not cause significant improvement in the compressive strength of unexposed geopolymer. Higher silica fume content of 4% reduced the compressive strength of the unexposed geopolymer. When subjected to elevated temperature, geopolymer with 2% silica fume retained higher compressive strength at 1000 °C. The addition of silica fume in fly ash geopolymer caused a lower degree of shrinkage and expansion, as compared to geopolymer without the addition of silica fume. Crystalline phases of albite and magnetite were formed in the geopolymer at 1000 °C.

Keywords: geopolymer; fly ash; amorphous; silica fume; thermal performance

Citation: Li, O.H.; Yun-Ming, L.; Cheng-Yong, H.; Bayuaji, R.; Abdullah, M.M.A.B.; Loong, F.K.; Jin, T.S.; Teng, N.H.; Nabiałek, M.; Jeż, B.; et al. Evaluation of the Effect of Silica Fume on Amorphous Fly Ash Geopolymers Exposed to Elevated Temperature. *Magnetochemistry* **2021**, *7*, 9. https://doi.org/10.3390/magnetochemistry7010009

Received: 28 November 2020
Accepted: 4 January 2021
Published: 6 January 2021

1. Introduction

Geopolymer is one of the alternatives to ordinary Portland cement (OPC), as a construction material, because it is more environmentally friendly [1,2]. The OPC production involves the burning of large amounts of fuel, thus resulting in almost 5% of total global CO_2 emissions [3]. Geopolymers are inorganic materials, introduced by Davidovits [4], and are made by mixing the solid aluminosilicate source with liquid alkaline activator, which is then cured at ambient temperature or a slightly higher temperature (<100 °C). The aluminosilicate sources, which consist of high silica and alumina, could be obtained from natural resources (kaolin and metakaolin) or industrial by-products (fly ash, bottom ash and rice husk ash). In addition, geopolymer could be used as an alternative to OPC because to its properties such as higher early strength, being superior against thermal resistance and lower CO_2 emission [5].

Geopolymers are generally recognized as superior systems with respect to thermal resistance. The amorphous aluminosilicate structure with three-dimensional arrangement

enables geopolymers to possess ceramic-like properties and exhibit high thermal resistant [6]. Studies have found that geopolymers are incombustible and do not spall with extended heating as geopolymer contains lower $Ca(OH)_2$ content in comparison to OPC [7]. Besides, geopolymers also exhibit superior thermal stability as no smokes or toxic gases are released when they are heated [8].

The excellent thermal stability of geopolymers not only increases its endurance at high temperature, but also alters its other properties and geopolymer structure. Deterioration of strength of geopolymer at elevated temperatures was commonly reported [9,10]. However, an increase in mechanical strength of geopolymer when exposed to elevated temperature has also been reported [11]. Park et al. [12] observed the occurrence of further geopolymerisation reaction in class F fly ash geopolymer at 400 °C, which leads to increasing strength. The compressive strength dropped at a temperature beyond 400 °C, as result of the initiation and propagation of thermal cracks. In contrast, Wongsa et al. [13] found that higher residual strength of fly ash geopolymers incorporating natural mullite and zeolite was achieved at 900 °C, which is associated with the increase in crystallinity of the matrix. Heat treatment would initiate phase transformation in a geopolymer matrix. Crystalline nepheline ($NaAlSiO_4$) is most reported in the heated geopolymer [14,15]. Based on Rovnaník and Safránková [15], albite ($NaAlSi_3O_8$) was also formed, except from nepheline, boosting the flexural strength of fly ash geopolymers. Payakaniti et al. [16] studied the relationship between thermal stability and the magnetic properties of high calcium fly ash geopolymer, and observed the formation of new phases of nepheline and zeolite and an increased hematite peak above 800 °C. The antiferromagnetic behaviour of hematite decreased the magnetic properties of geopolymers and eventually switched from ferromagnetic to paramagnetic properties when the temperature reached 1200 °C.

The incorporation of nanoparticles leads to the enhancement of physical structure and mechanical strength of geopolymer matrices. Silica fume is one of the potential nanoparticles that could be introduced into geopolymer as it is a highly effective pozzolanic and possesses extreme fineness and high silica content [17]. Incorporation of silica fume induces Si content, which improves the yield of geopolymer gels and results in a strength increment [18–21] with lower porosity and water absorption [22,23]. Liu et al. [21] reported superior compressive strength of 151 MPa when 30% of silica fume was incorporated into the fly ash/slag geopolymer concretes. It has been proven that the addition of silica fume results in improvement of mechanical strength, durability, and structure properties of geopolymers. Despite understanding the thermal resistance of pure geopolymers without additives, and the mechanical strength development of geopolymer with silica fume addition, the influence of silica fume on the properties of geopolymers at elevated temperatures is not known. The past literature mostly covers the evolution of microstructure and mechanical strength under the influence of a silica additive.

Therefore, this paper evaluates and compares the effect of the addition of silica fume on physical, mechanical properties and thermal resistance of fly ash geopolymers. A quantitative research study was performed on fly ash geopolymer with varying dosages of silica fume (0%, 2%, and 4%).

2. Methodology

2.1. Materials

The Class F fly ash used in this work was sourced from Manjung Coal-Fired Power Plant, Perak. The chemical composition of the fly ash is displayed in Table 1. The fly ash is made up mainly of SiO_2 (56.3%) and Al_2O_3 (28.0%). Figure 1a demonstrates that the fly ash is highly amorphous with some crystalline inclusions of quartz, mullite and hematite. The fly ash particles revealed in Figure 1b have spherical shapes with smooth surfaces and wide size distributions.

Table 1. Chemical composition of Class F fly ash determined using X-ray Fluorescence (XRF).

Compound	SiO_2	Al_2O_3	Fe_2O_3	CaO	Others
Mass (%)	56.3	28.0	6.86	3.89	4.95

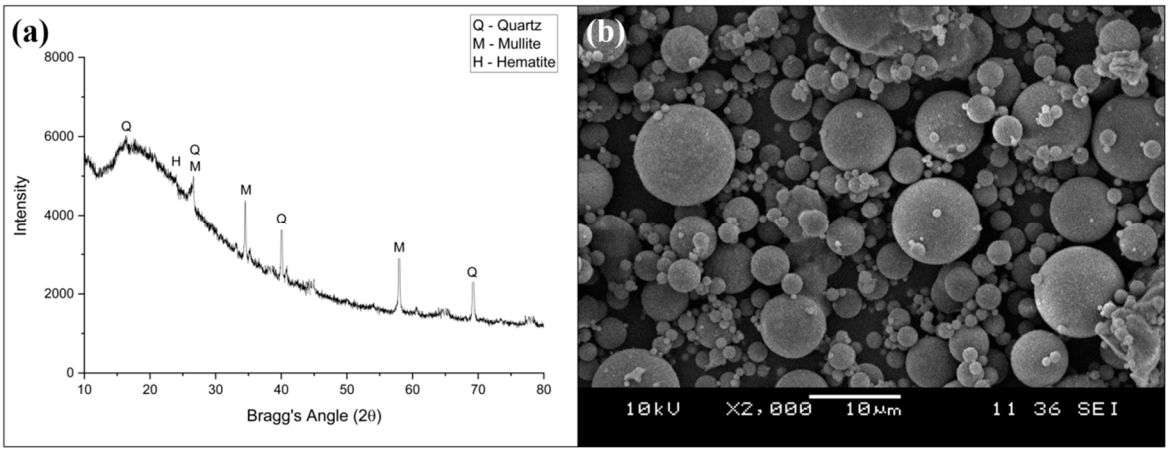

Figure 1. (**a**) XRD diffractogram and (**b**) Scanning electron microscope (SEM) micrograph of Class F fly ash.

Sodium hydroxide (NaOH) pellets with an assay (total alkalinity calculated as NaOH) of 98.0–100.5% were supplied by Progressive Scientific Sdn. Bhd., Selangor. Technical grade liquid sodium silicate (Na_2SiO_3) with 60.5% H_2O, 30.1% SiO_2 and 9.4% Na_2O with 3.2 SiO_2/Na_2O ratios was supplied by South Pacific Chemicals Industries (SPCI) Sdn. Bhd., Malaysia. Nano-silica (silica fume) with an average particle size of 7 nm, surface area of 395 ± 25 m^2/g and density of 36.8 kg/m^3, supplied by Sigma-Aldrich Corporation, was added into fly ash geopolymers as the additive.

2.2. Geopolymer Formation

The binder-to-liquid ratio and Na_2SiO_3/NaOH ratio was fixed at 2.0 and 2.5, respectively, for the geopolymer mixture. The alkali activator was prepared by mixing NaOH 10 M solution with liquid Na_2SiO_3. Silica fume was first dry mixed with fly ash and then mixed with the alkali activator to achieve homogeneous slurry. The silica fume was added in 0%, 2% and 4% by weight of fly ash. The slurry was casted in molds with dimensions of 50 × 50 × 50 mm and then compacted to remove the entrapped air. The samples were first cured at room temperature (29 °C) for 24 h before oven-curing at 60 °C for another 24 h. This curing regime was selected as pre-curing at room temperature, followed by oven-curing, which are beneficial for strength improvement, based on Ranjbar et al. work [24]. After the curing process, the hardened geopolymer samples were sealed and kept under room temperature for 28 days.

2.3. Heat Treatment

The 28 day cured fly ash geopolymers were heat-treated in a furnace at 200 °C, 600 °C and 1000 °C, with a heating rate of 5 °C/min for 2 h. A set of geopolymer samples was left unexposed for comparison purposes.

2.4. Testing, Analysis and Characterization Method

The density of geopolymers was calculated by measuring the dimension and mass of the samples before and after exposure to elevated temperature, in accordance with ASTM C138/C138M. Compressive test was accessed according to ASTM C109/C109M by using universal testing machine (UTM) modeled Shimadzu UH-1000 kNI. The loading rate was fixed constant at 5 mm/min. Three samples were compressed to obtain the average strength value. The microstructure of fly ash and fly ash geopolymers were revealed with

scanning electron microscopy (SEM) modeled JEOL JSM-6460 LA. Perkin Elmer Fourier Transform Infrared Spectroscopy (FTIR) was used to analyze the functional group of fly ash, fly ash geopolymer and bond vibration frequencies. The samples were scanned from 650 cm^{-1} to 4000 cm^{-1} with a resolution of 4 cm^{-1}. X-ray diffraction (XRD) was performed to characterize the mineralogical changes using Shimadzu X-ray Diffractometer modeled XRD-6000. To investigate the shrinkage or expansion of fly ash geopolymer samples, LINSEISL76 Platinum Series dilatometer was used to investigate its thermal properties.

3. Results and Discussion

3.1. Physical Observation

Figure 2 displays the surface conditions of unexposed fly ash geopolymers with varying contents of silica fume. It could be clearly seen that more pores were found on the surface of geopolymer without the addition of silica fume (Figure 2a). However, porosity of geopolymer decreased as the content of silica fume increased. Silica fume behaved as a pore-filler as it had a very fine particle size [19], which could fill the empty space within the geopolymer matrix. In addition, some visible white spots could be observed on the surface of geopolymers, which was known as the efflorescence effect [25].

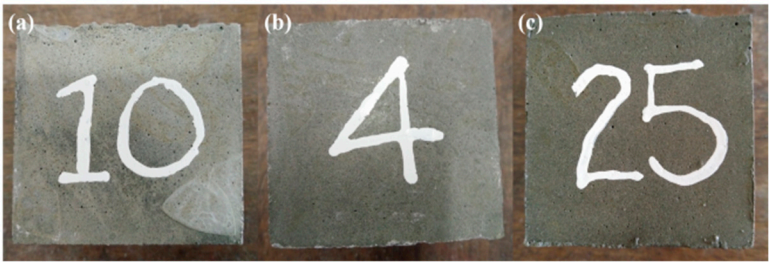

Figure 2. Physical appearances of unexposed fly ash geopolymers with (**a**) 0%, (**b**) 2% and (**c**) 4% of silica fume.

Figure 3 depicts the physical appearances of exposed fly ash geopolymers with a different percentage of silica fume addition. In general, the color changed from dark grey to light grey when heated to 200 °C (Figure 3b), while it further changed to beige when exposed to 60 °C (Figure 3c). The color changes at 60 °C were mainly associated with the oxidation changes of iron oxide content in fly ash [26]. Moreover, the color of the sample further changed to dark brown at 1000 °C (Figure 3d), which was related to the recrystallisation of the amorphous phase in the geopolymer matrix [27].

However, there were severe cracks observed in geopolymer without additive, whereby minor cracks observed in the geopolymer with silica fume addition at 1000 °C. It is suggested that, by the incorporation of silica fume, it tended to solve the problem of cracks with only a small amount (2% and 4%) of silica fume.

Figure 3. Physical appearance of fly ash geopolymers with varying silica fume content: (**a**) unexposed; (**b**) 200 °C; (**c**) 600 °C; and (**d**)1000 °C.

3.2. Density Measurement

Figure 4 illustrates the density changes of fly ash geopolymers with varying percentages of silica fume at elevated temperatures. In general, the change in density of unexposed geopolymer, regardless of the addition of silica fume, was not significant. The unexposed geopolymer had a density of 1844.6 kg/m^3. Increasing silica fume content up to 2% slightly raised the density to 1893.2 kg/m^3. Inclusion of silica fume enhanced the geopolymerisation reaction due to the induced Si content, which rendered more reaction products and hence increased density. The observation was supported by Adak et al. [18]. The density decreased to 1875.6 kg/m^3 with 4% of silica fume, which was associated with the hindered geopolymerisation reaction at high silica contents. When excess silica content reacted with insufficient alumina content, the reaction products and the density reduced. It was further supported by Ghanbari et al. [28] who produced a metakaolin geopolymer with the addition of silica fume.

In the case of exposed geopolymers, all geopolymers displayed a reduction trend in the density with increasing temperature. The density loss corresponded to the mass loss in geopolymer during sintering. Mass loss is linked with the moisture loss of chemically and physically bonded water below 600 °C [29]. In comparison, the density loss of geopolymers without silica fume (9.3–28.1%) was higher than the geopolymer with silica fume addition (5.8–27.6%). This was because the geopolymers without silica fume (10.4–21.7%) have higher mass loss than the geopolymer with silica fume addition (11–20.7%). It meant that, by the inclusion of silica fume, it reduced the mass loss of geopolymers and hence resulted in reduced density loss.

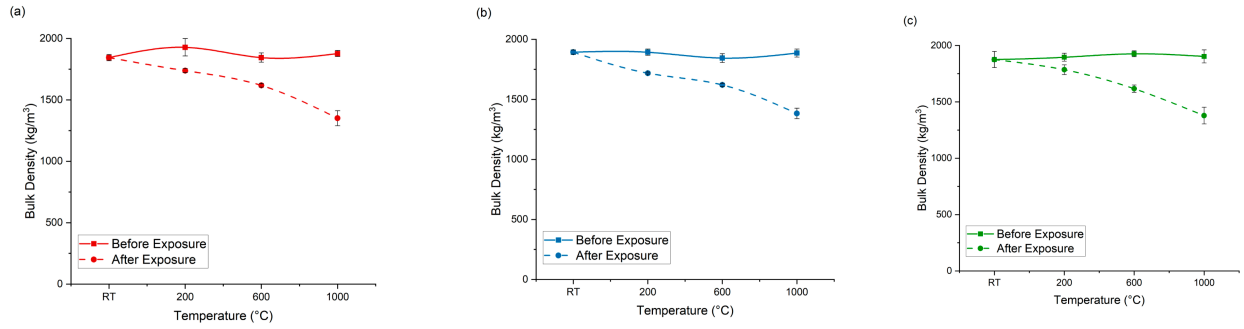

(**a**) (**b**) (**c**)

Figure 4. Density of fly ash geopolymers with (**a**) 0%, (**b**) 2%, and (**c**) 4% of silica fume before and after exposure to elevated temperature.

3.3. Compressive Strength Test

Figure 5 shows the compressive strength evolution of fly ash geopolymer before and after being exposed to elevated temperatures. Unexposed geopolymers without silica fume attained a compressive strength of 14.3 MPa. Incorporation of 2% of silica fume did not significantly improve the compressive strength (14.5 MPa), despite the reduced observable pores and increased density, as shown in Figures 2 and 4, respectively. However, obvious degradation of compressive strength to 8.6 MPa was recorded for the geopolymer with 4% silica fume. This could be due to the increased workability of geopolymer mixture at higher silica fume content. The observation was supported by Das et al. [30], who reported a reduction of compressive strength due to increased flowability with increasing silica fume from 1% to 3%. Increased workability restricted the contact between the aluminosilicate and alkali activator.

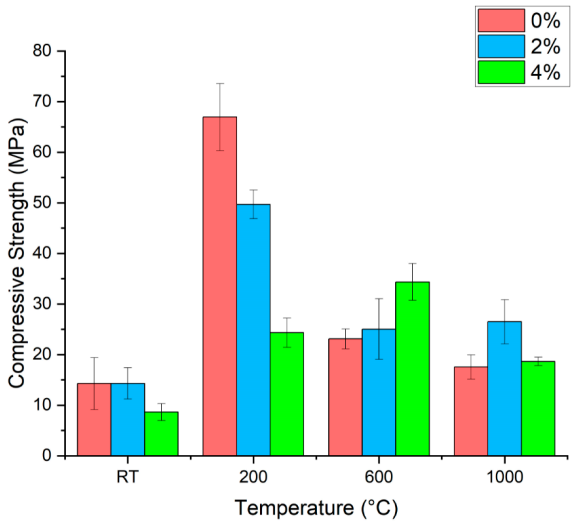

Figure 5. Compressive strength of fly ash geopolymers with varying silica fume content before and after exposure to elevated temperatures.

In the case of exposed geopolymer without silica fume, increasing temperature raised its compressive strength up to 200 °C (67 MPa) and the strength reduced after 200 °C. The reason of the strength gained at 200 °C was related to the quicker of geopolymerisation reaction as temperature of 200 °C could stiffen the binder at a faster rate [31]. The compressive strength dropped above 200 °C and was associated with the high-density loss (Figure 4) and crack formation (Figure 3). Particularly at 1000 °C, the geopolymer samples exhibited wide visible cracks and the highest density loss (28.1%). The formation of crack

would destroy the sample and hence be unbeneficial to the strength performance of the geopolymer.

Geopolymer with 2% silica fume also possessed compressive strength increment up to 49.7 MPa at 200 °C. The compressive strength further reduced to 25.0 MPa at 600 °C. At 1000 °C, the compressive strength remained (26.5 MPa), which might be due to the crystalline phase formation [27]. However, for the geopolymer with 4% silica fume, the compressive strength increased up to 24.3 MPa at 200 °C, 34.3 MPa at 600 °C and further reduced to 18.7 MPa at 1000 °C. The sharp spike in the compressive strength at 200 °C, regardless of the addition of silica fume, was mainly due to the quasi equilibrium of geopolymerisation reaction under room temperature. Thus, when heat was applied, the temperature-controlled dissolution and geopolymerisation occurred and consequently enhanced the compressive strength of the final products [24]. This subsequently caused the further increment in the compressive strength of geopolymer with 4% silica fume up to 600 °C. The higher silica content tended to slow down the kinetics of geopolymerisation reaction [24] and hence a higher temperature was required to improve the mechanical strength. The strength reduction at 1000 °C for geopolymer with 4% silica fume was due to the higher degree of expansion, which will be discussed in the next section.

In summary, the strength retention of geopolymer with 2% of silica fume at elevated temperature proved that addition of a low amount of silica fume helped to improve the thermal stability of the geopolymer.

3.4. Thermal Shrinkage and Expansion Measurement

Figure 6 depicts the dilatometry performance of fly ash geopolymers with varying silica fumes up to 1000 °C. Geopolymers without silica fume shrunk from room temperature to 700 °C and then expanded up to 1000 °C. Similar trend was observed for geopolymer with the addition of silica fume up to 800 °C. Beyond 800 °C, shrinkage was observed. In general, the dilatometric curves of geopolymers can be divided into three zones. The first zone (up to 300 °C) was due to the establishment of capillary contraction when the water was evaporated. The second zone (300 °C–700 °C) was associated with the dehydroxylation reaction. The third zone (700 °C–1000 °C) corresponded to the viscous sintering effect and phase transformation.

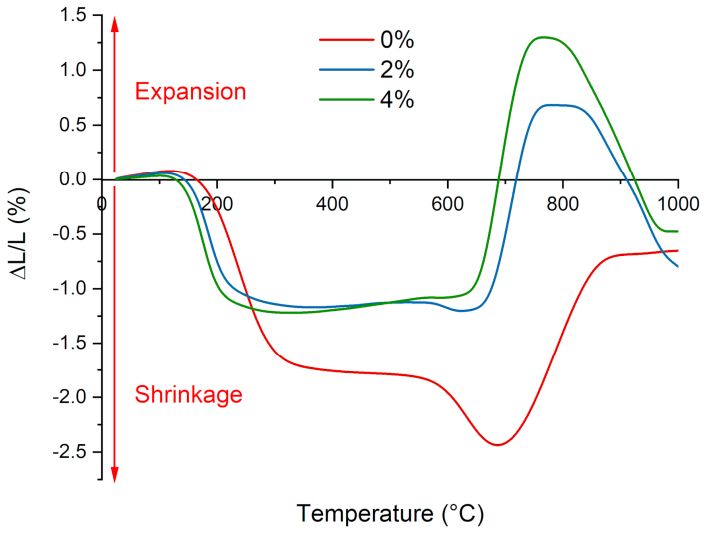

Figure 6. Dilatometry curves of fly ash geopolymers with varying silica fume content from room temperature to 1000 °C.

As seen from Figure 6, the geopolymer with silica fume content shrunk at a slightly lower temperature than the geopolymer without silica fume. This was related to the very fine particle of silica fume, which could strengthen the formation of rings and chains of

polysialates that shrink by 100 °C. The degree of shrinkage of geopolymer up to 700 °C with silica fume was lower compared to the reference geopolymer (without silica fume). In the contrary, in the temperature range of 600 to 800 °C, the expansion of geopolymer with 2% silica fume was the lowest compared to the counterpart without silica fume and with 4% of silica fume, which consequently caused the highest strength attained for geopolymer with 2% silica fume, as shown in Figure 5. The higher degree of expansion of geopolymer without silica fume and with 4% silica fume was the most probable reason for strength reduction at 1000 °C.

3.5. Phase Identification

Figure 7 illustrates the phase identification of unexposed fly ash geopolymers with varying percentages of silica fume. Geopolymers are highly amorphous. The existence of main crystalline phases of mullite and quartz and minor hematite phase in geopolymer was originated from fly ash (Figure 1a). However, a new crystalline phase of zeolite appeared in the geopolymer. The zeolite formation was recognized as the secondary reaction products during the geopolymerisation process in accordance with Rashad and Zeedan [32]. It is observed that the intensity of mullite and quartz (26.5° 2θ) was high in the geopolymer with 4% of silica fume. The high content entailed that lower dissolution of aluminosilicate and progress of chemical reaction to form the geopolymer network, as aforementioned, and prove the low compressive strength of the geopolymer with 4% of silica fume.

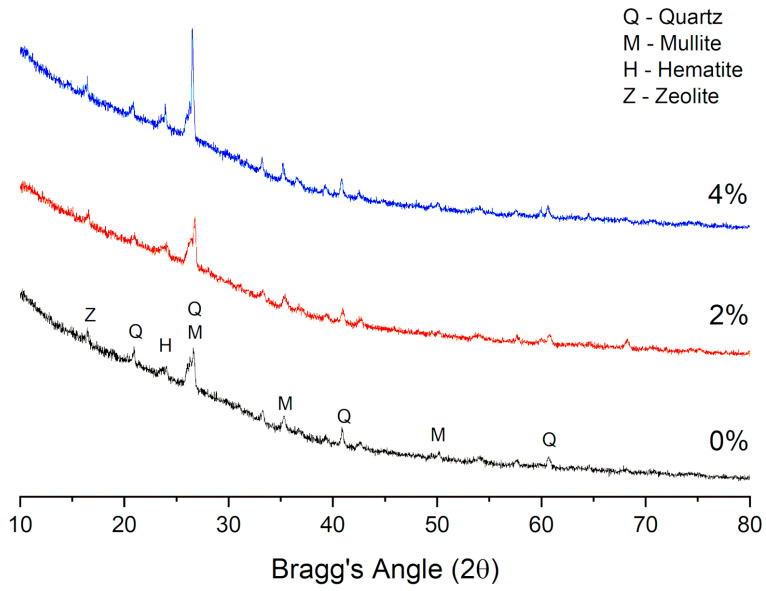

Figure 7. XRD patterns of unexposed fly ash geopolymers with varying silica fume contents.

Figure 8 displays the phase analysis of exposed fly ash geopolymers. The diffraction peaks of quartz and mullite at 26.5° 2θ remained in the geopolymers, even though they were heated to elevated temperatures, which verified that they were highly stable. Quartz and mullite did not decompose below a temperature of 1000 °C as they have a high melting point of 1840 °C and 1670 °C, respectively. Besides, a minor peak of hematite disappeared at 1000 °C was believed to be transformed into magnetite at 600 °C, which leads to the beige color appearance of the geopolymer sample (Figure 3c). The occurrence of this conversion process was common under elevated temperature [33]. A new crystalline peak of albite appeared at 1000 °C. The presence of albite was supposed to retain the compressive strength of geopolymer at an elevated temperature, as supported by Alehyen et al. [27].

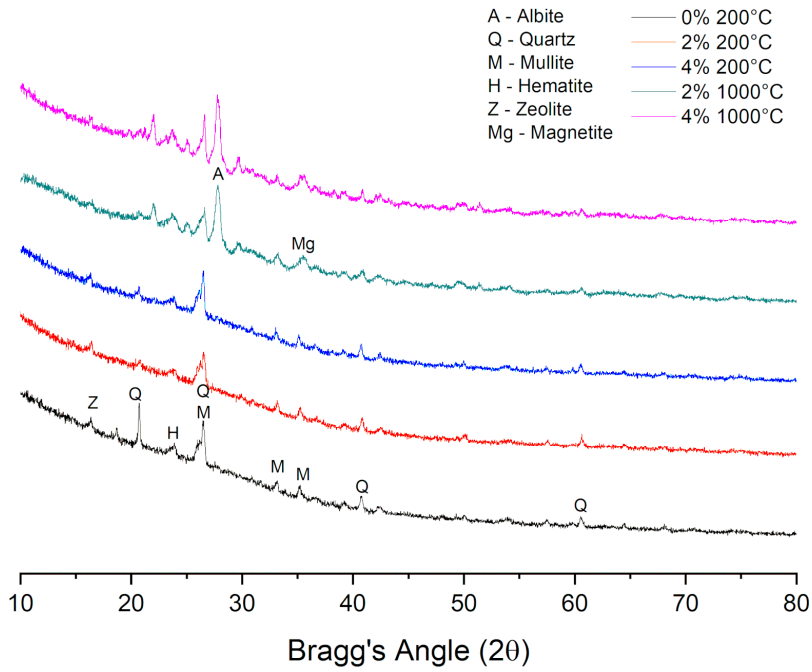

Figure 8. XRD patterns of fly ash geopolymers with varying silica fume content addition after being exposed to 200 °C and 1000 °C.

3.6. Functional Group Identification

Figure 9 depicts the IR spectrum of fly ash. The main band (1029 cm^{-1}) and a minor band (729 cm^{-1}) were recognized as asymmetric stretching vibration (Si-O-Si and Si-O-Al) [34] and symmetric stretching vibration (Si-O-Si) [35], respectively. Another band of 2348 cm^{-1} was assigned as symmetric axial deformation of the CO_2 [36], whereby the region at 1529 cm^{-1} was verified as the stretching vibration (C-O) [37]. In addition, the bands of 3608 cm^{-1} and 1694 cm^{-1} were assigned as OH stretching [38] and bending [39] vibrations, respectively.

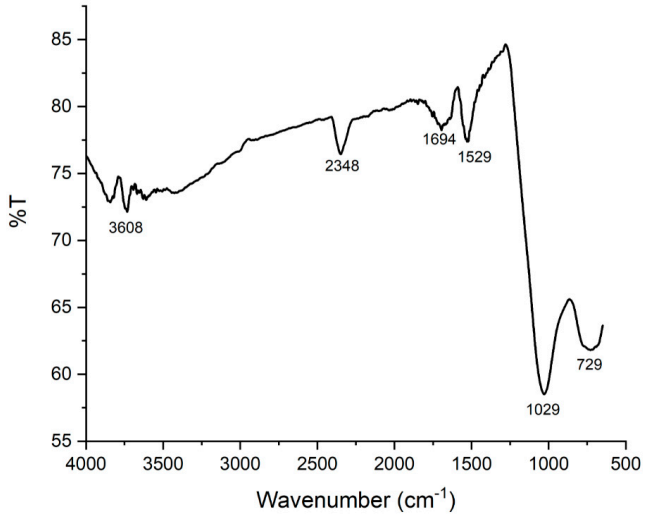

Figure 9. Infrared (IR) spectrum of fly ash.

Figure 10 represents the IR spectra of unexposed fly ash geopolymers with different contents of silica fume. The absorption bands of geopolymer were almost similar with fly ash (Figure 9). The additional band at ~3300 cm^{-1} was also corresponded to the O-H stretching vibration [38]. The main band of fly ash at 1029 cm^{-1} shifted to a lower wavenumber

(~980 cm^{-1}). The shift implied that the formation of amorphous aluminosilicate gel phase after the activation of fly ash amorphous phase by alkali solution [38].

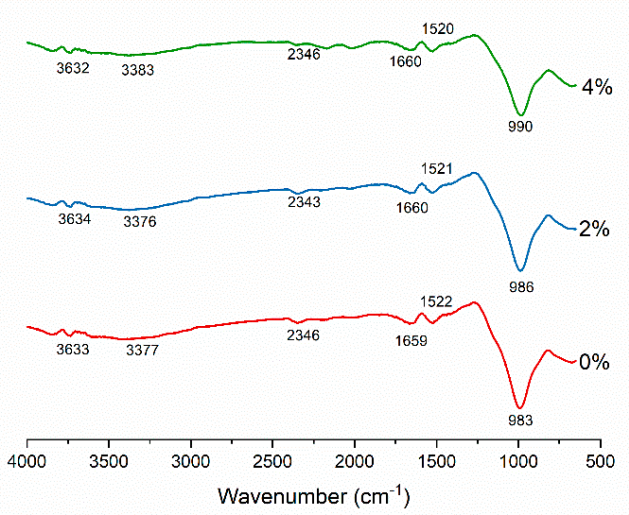

Figure 10. IR spectra of un-exposed fly ash geopolymers with varying silica fume content addition.

The addition of silica fume did not alter or produce a new absorption band in geopolymer. Increasing the silica fume content increased the wavenumber from 983 cm^{-1} to 990 cm^{-1}, associated with the formation of geopolymer network that is rich in Si bonds [40]. The intensity of this band for the reference geopolymer and geopolymer with 2% silica fume is almost similar, while the intensity reduced (higher percentage transmittance) in geopolymer with 4% silica fume. The observation complied with the compressive strength result in Figure 5, whereby the compressive strength of geopolymer with 4% silica fume was lower than the counterpart with no silica fume and 2% of silica fume.

When subjected to 200 °C (Figure 11), increasing silica fume content up to 4%, the intensity of the band at ~980 cm^{-1} decreased with increasing silica fume content, which was also consistent with the recorded compressive strength, as shown in Figure 5. However, at 1000 °C, the geopolymer with 2% silica fume has the highest intensity of this band due to increased Si-O-Al bonds which were further verified by the phase identification (Figure 8) as albite ($NaAlSi_3O_8$) was formed at 1000 °C in addition to the sodium aluminium silicate hydrate (N-A-S-H).

In addition, as referred to in Figure 11, the absorption bands due to OH stretching vibration (~3300–33,600 cm^{-1}) and OH bending vibration (~1630 cm^{-1}) reduced in intensity at high temperature exposure. The indicated the dehydration of structure with increasing temperature. The intensity of C-O bonds at ~2340 cm^{-1} and ~1470 cm^{-1} also reduced due to the breakage of C-O at elevated temperatures. Based on Figures 10 and 11, there are differences in the intensity of bands at ~3300 cm^{-1} and ~1630 cm^{-1} of the unexposed and exposed geopolymer samples. It was supposed that the intensity of these bands was higher in the unexposed samples compared to those that were exposed to elevated temperatures. The discrepancy of result was due to the different stages of experimental work done. Therefore, the comparison of the bands between unexposed and exposed geopolymer samples was not discussed.

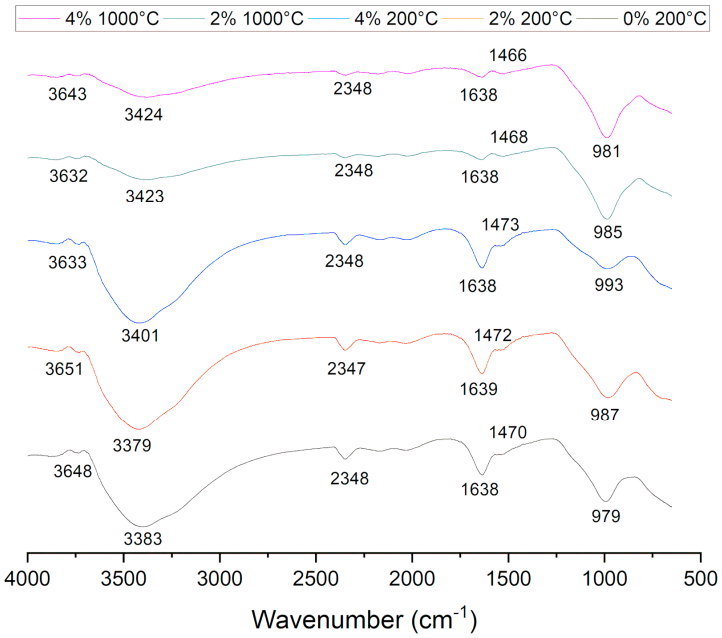

Figure 11. IR spectra of fly ash geopolymers with varying silica fume content addition after being exposed to 200 °C and 1000 °C.

3.7. Microstructural Analysis

Figure 12 illustrates the SEM micrographs of unexposed fly ash geopolymers with varying silica fume contents under magnification of 1000×. In general, some remnant fly ash particles indicated by the spherical particles with smooth surface, pores and cracks were observed in the matrix of all geopolymers. The reference geopolymer revealed a relatively loose matrix and some microcracks (Figure 12a). With the addition of 2% silica fume (Figure 12b), the microstructure became denser and homogeneous with less unreacted fly ash. Yet, the microstructure of the geopolymer with 4% of silica fume was comprised of a loose microstructure with a large amount of unreacted fly ash and wider cracks (Figure 12c).

Figure 13 illustrates the SEM micrographs of exposed fly ash geopolymers (magnification 500×). Exposure to high temperature led to transformation in the microstructure of geopolymers and affected its mechanical strength. Based on Figure 13a, the geopolymer matrix was dense, with fewer cracks, remnant fly ash particles and pores after being exposed to 200 °C. Therefore, the dense microstructure contributed to the improvement of compressive strength of the geopolymer at 200 °C (Figure 5). However, with increasing temperature up to 1000 °C, solidifying melt occurred and intervening matrix was observed. At the same time, large pores were observed in the exposed geopolymer to 1000 °C. This might be the reason for the degradation in the compressive strength at high temperature. The observation was supported by Škvára et al. [41] when subjected to fly ash geopolymer to high temperatures. Referring to Figure 13, the geopolymer with 4% silica fume was comprised of larger pores and hence recorded lower compressive strength than geopolymer with 2% silica fume.

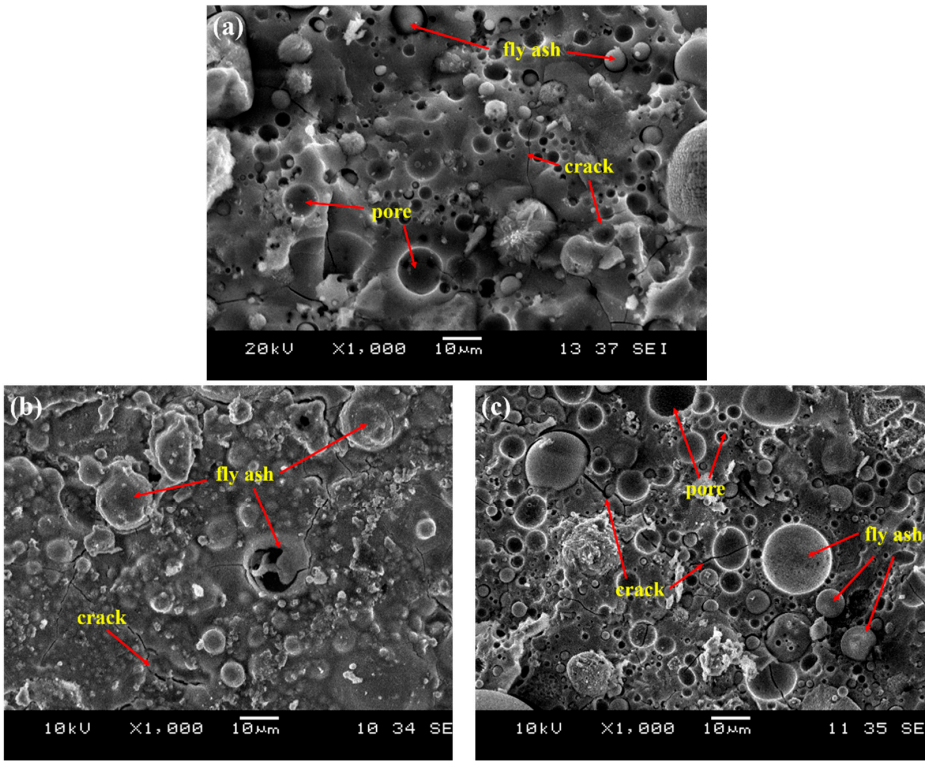

Figure 12. SEM micrographs of fly ash geopolymers with (**a**) 0%, (**b**) 2% and (**c**) 4% of silica fume.

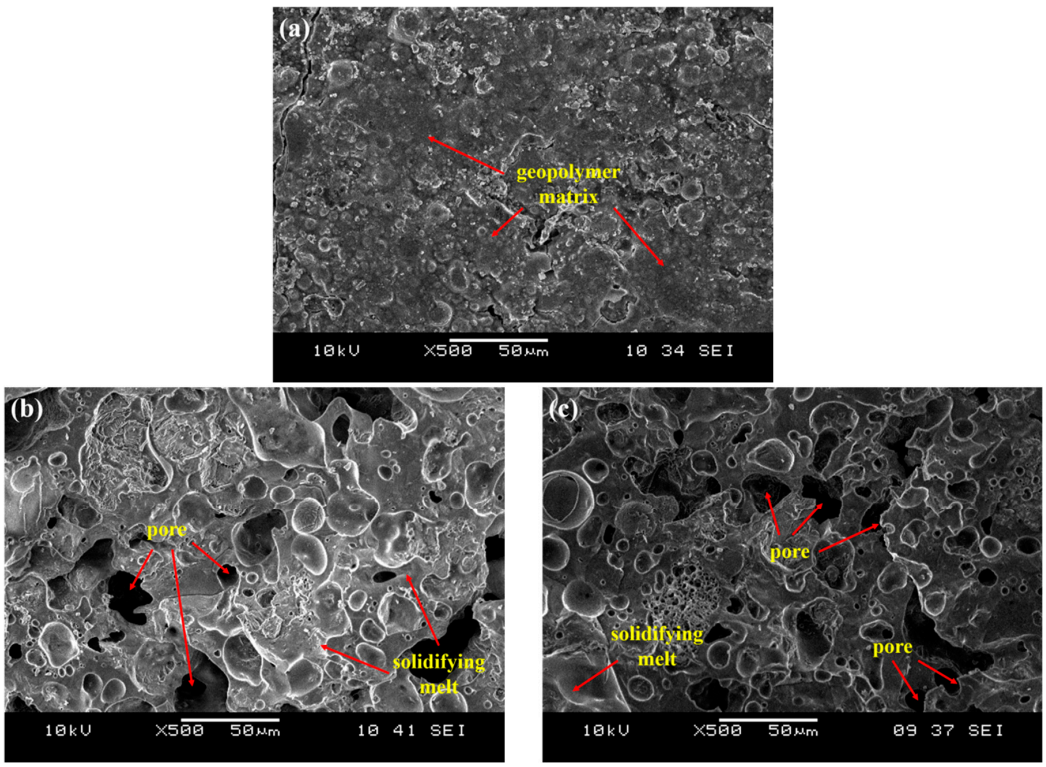

Figure 13. SEM micrographs of fly ash geopolymers with (**a**) 2% of silica fume addition after exposed to 200 °C, (**b**) 2% and (**c**) 4% of silica fume addition after exposed to 1000 °C.

4. Conclusions

This paper investigated the influence of silica fume on the thermal performance of fly ash geopolymers. The addition of silica fume (2%) did not boost up the compressive strength of fly ash geopolymer, while higher silica fume content of 4% degraded the compressive strength due to the impeded dissolution and geopolymerisation reaction. In general, all exposed geopolymers, regardless of the addition of silica fume, showed improvement in strength at 200 °C and then deterioration of strength with further increase in exposed temperature. Even so, the addition of 2% silica fume showed no degradation of compressive strength at 1000 °C compared to that exposed to 600 °C. In addition, the extent of shrinkage and expansion of geopolymers with 2% silica fume was the lowest among all geopolymers, which showed the improvement of thermal stability of geopolymer due to effect of silica fume. Albite and magnetite peaks were formed in the geopolymer with silica fume at 1000 °C and the intervening matrix was produced due to partial melting at high temperature.

Author Contributions: Conceptualization, L.Y.-M. and H.C.-Y.; synthesis of samples, O.H.L.; Supervision, L.Y.-M. and H.C.-Y.; writing-original draft preparation, O.H.L.; writing-review and editing, L.Y.-M., N.H.T. and N.Y.S.; Resources, R.B., M.M.A.B.A., F.K.L. and T.S.J.; Validation, M.N. and B.J. All authors have read and agreed to the published version of the manuscript.

Funding: This research received no external funding.

Institutional Review Board Statement: Not applicable.

Informed Consent Statement: Not applicable.

Data Availability Statement: The data presented in this study are available in this article.

Acknowledgments: The authors of the present work wish to acknowledge the support from Faculty of Chemical Engineering Technology, Universiti Malaysia Perlis (UniMAP) for the laboratory facilities throughout the project.

Conflicts of Interest: The authors declare no conflict of interest.

References

1. Pavithra, P.; Srinivasula Reddy, M.; Dinakar, P.; Hanumantha Rao, B.; Satpathy, B.K.; Mohanty, A.N. A mix design procedure for geopolymer concrete with fly ash. *J. Clean. Prod.* **2016**, *133*, 117–125. [CrossRef]
2. Mesgari, S.; Akbarnezhad, A.; Xiao, J. Recycled geopolymer aggregates as coarse aggregates for Portland cement concrete and geopolymer concrete: Effects on mechanical properties. *Constr. Build. Mater.* **2020**, *236*, 117571. [CrossRef]
3. Chiniforush, A.A.; Xiao, J. Estimation and Minimization of Embodied Carbon of Buildings: A Review. *Buildings* **2017**, *7*, 5.
4. Davidovits, J. Geopolymers: Ceramic-like inorganic polymers. *J. Ceram. Sci. Technol.* **2017**, *8*, 335–350.
5. Shaikh, F.U.A. Mechanical and durability properties of fly ash geopolymer concrete containing recycled coarse aggregates. *Int. J. Sustain. Built Environ.* **2016**, *5*, 277–287. [CrossRef]
6. Ogundiran, M.B.; Kumar, S. Synthesis of fly ash-calcined clay geopolymers: Reactivity, mechanical strength, structural and microstructural characteristics. *Constr. Build. Mater.* **2016**, *125*, 450–457. [CrossRef]
7. Sturm, P.; Gluth, G.; Simon, S.; Brouwers, H.J.H.; Kühne, H.-C. The effect of heat treatment on the mechanical and structural properties of one-part geopolymer-zeolite composites. *Thermochim. Acta* **2016**, *635*, 41–58. [CrossRef]
8. Zhang, H.Y.; Kodur, V.; Wu, B.; Yan, J.; Yuan, Z.S. Effect of temperature on bond characteristics of geopolymer concrete. *Constr. Build. Mater.* **2018**, *163*, 277–285. [CrossRef]
9. Heah, C.Y.; Yun-Ming, L.; Abdullah, M.M.A.B.; Hussin, K. Thermal Resistance Variations of Fly Ash Geopolymers: Foaming Responses. *Sci. Rep.* **2017**, *7*, srep45355.
10. Zhang, H.Y.; Kodur, V.; Qi, S.L.; Cao, L.; Wu, B. Development of metakaolin–fly ash based geopolymers for fire resistance applications. *Constr. Build. Mater.* **2014**, *55*, 38–45. [CrossRef]
11. Miltiadis, S.K.; Panias, D.; Nomikos, P.; Sofianos, A. Potassium based geopolymer for passive fire protection of concrete tunnels linings. *Tunn. Undergr. Space Technol.* **2014**, *43*, 148–156.
12. Lee, H.; Jang, J.; Lee, N.; Lee, H. Physicochemical properties of binder gel in alkali-activated fly ash/slag exposed to high temperatures. *Cem. Concr. Res.* **2016**, *89*, 72–79.
13. Wongsa, A.; Wongkvanklom, A.; Tanangteerapong, D.; Chindaprasirt, P. Comparative study of fire-resistant behaviors of high-calcium fly ash geopolymer mortar containing zeolite and mullite. *J. Sustain. Cem. Mater.* **2020**, *9*, 307–321.

14. Ranjbar, N.; Mehrali, M.; Alengaram, U.J.; Metselaar, H.S.C.; Jumaat, M.Z. Compressive strength and microstructural analysis of fly ash/palm oil fuel ash based geopolymer mortar under elevated temperatures. *Constr. Build. Mater.* **2014**, *65*, 114–121. [CrossRef]
15. Rovnaník, P.; Šafránková, K. Thermal Behaviour of Metakaolin/Fly Ash Geopolymers with Chamotte Aggregate. *Materials* **2016**, *9*, 535. [CrossRef] [PubMed]
16. Payakaniti, P.; Chuewangkam, N.; Yensano, R.; Pinitsoontorn, S.; Chindaprasirt, P. Changes in compressive strength, microstructure and magnetic properties of a high-calcium fly ash geopolymer subjected to high temperatures. *Constr. Build. Mater.* **2020**, *265*, 120650. [CrossRef]
17. Lee, N.K.; An, G.H.; Koh, K.T.; Ryu, G.S. Improved Reactivity of Fly Ash-Slag Geopolymer by the Addition of Silica Fume. *Adv. Mater. Sci. Eng.* **2016**, *2016*, 1–11. [CrossRef]
18. Adak, D.; Sarkar, M.; Mandal, S. Structural performance of nano-silica modified fly-ash based geopolymer concrete. *Constr. Build. Mater.* **2017**, *135*, 430–439. [CrossRef]
19. Duan, P.; Yan, C.; Zhou, W. Compressive strength and microstructure of fly ash based geopolymer blended with silica fume under thermal cycle. *Cem. Concr. Compos.* **2017**, *78*, 108–119. [CrossRef]
20. Saini, G.; Vattipalli, U. Assessing properties of alkali activated GGBS based self-compacting geopolymer concrete using nano-silica. *Case Stud. Constr. Mater.* **2020**, *12*, e00352. [CrossRef]
21. Liu, Y.; Shi, C.; Zhang, Z.; Li, N.; Shi, D. Mechanical and fracture properties of ultra-high performance geopolymer concrete: Effects of steel fiber and silica fume. *Cem. Concr. Compos.* **2020**, *112*, 103665. [CrossRef]
22. Adak, D.; Sarkar, M.; Mandal, S. Effect of nano-silica on strength and durability of fly ash based geopolymer mortar. *Constr. Build. Mater.* **2014**, *70*, 453–459. [CrossRef]
23. Khater, H.M. Effect of nano-silica on microstructure formation of low-cost geopolymer binder. *Nanocomposites* **2016**, *2*, 84–97. [CrossRef]
24. Ranjbar, N.; Kuenzel, C.; Spangenberg, J.; Mehrali, M. Hardening evolution of geopolymers from setting to equilibrium: A review. *Cem. Concr. Compos.* **2020**, *114*, 103729. [CrossRef]
25. Zhang, Z.; Provis, J.L.; Reid, A.; Wang, H. Fly ash-based geopolymers: The relationship between composition, pore structure and efflorescence. *Cem. Concr. Res.* **2014**, *64*, 30–41. [CrossRef]
26. Temuujin, J.; Van Riessen, A. Effect of fly ash preliminary calcination on the properties of geopolymer. *J. Hazard. Mater.* **2009**, *164*, 634–639. [CrossRef]
27. Alehyen, S.; Zerzouri, M.; el Alouani, M.; el Achouri, M.; Taibi, M. Porosity and fire resistance of fly ash based geopolymer. *J. Mater. Environ. Sci.* **2017**, *8*, 3676–3689.
28. Ghanbari, M.; Hadian, A.; Nourbakhsh, A.; MacKenzie, K. Modeling and optimization of compressive strength and bulk density of metakaolin-based geopolymer using central composite design: A numerical and experimental study. *Ceram. Int.* **2017**, *43*, 324–335. [CrossRef]
29. Yang, Z.; Mocadlo, R.; Zhao, M.; Sisson, R.D.; Tao, M.; Liang, J. Preparation of a geopolymer from red mud slurry and class F fly ash and its behavior at elevated temperatures. *Constr. Build. Mater.* **2019**, *221*, 308–317. [CrossRef]
30. Das, S.K.; Mustakim, S.M.; Adesina, A.; Mishra, J.; Alomayri, T.S.; Assaedi, H.S.; Kaze, C.R. Fresh, strength and microstructure properties of geopolymer concrete incorporating lime and silica fume as replacement of fly ash. *J. Build. Eng.* **2020**, *32*, 101780. [CrossRef]
31. Pan, Z.; Sanjayan, J.G.; Collins, F. Effect of transient creep on compressive strength of geopolymer concrete for elevated temperature exposure. *Cem. Concr. Res.* **2014**, *56*, 182–189. [CrossRef]
32. Rashad, M.; Zeedan, S.R. The effect of activator concentration on the residual strength of alkali-activated fly ash pastes subjected to thermal load. *Constr. Build. Mater.* **2011**, *25*, 3098–3107. [CrossRef]
33. Ponomar, V.; Brik, O.; Cherevko, Y.; Ovsienko, V. Kinetics of hematite to magnetite transformation by gaseous reduction at low concentration of carbon monoxide. *Chem. Eng. Res. Des.* **2019**, *148*, 393–402. [CrossRef]
34. Liu, Y.; Zhu, W.; Yang, E.-H. Alkali-activated ground granulated blast-furnace slag incorporating incinerator fly ash as a potential binder. *Constr. Build. Mater.* **2016**, *112*, 1005–1012. [CrossRef]
35. Peyne, J.; Gautron, J.; Doudeau, J.; Joussein, E.; Rossignol, S. Influence of calcium addition on calcined brick clay based geopolymers: A thermal and FTIR spectroscopy study. *Constr. Build. Mater.* **2017**, *152*, 794–803. [CrossRef]
36. Pereira, A.P.D.S.; Da Silva, M.H.P.; Lima, E.P., Jr.; Paula, A.D.S.; Tommasini, F.J. Processing and Characterization of PET Composites Reinforced with Geopolymer Concrete Waste. *Mater. Res.* **2017**, *20*, 411–420. [CrossRef]
37. Yuan, B.; Yu, Q.; Brouwers, H.J.H. Reaction kinetics, reaction products and compressive strength of ternary activators activated slag designed by Taguchi method. *Mater. Des.* **2015**, *86*, 878–886. [CrossRef]
38. Prusty, J.K.; Pradhan, B. Multi-response optimization using Taguchi-Grey relational analysis for composition of fly ash-ground granulated blast furnace slag based geopolymer concrete. *Constr. Build. Mater.* **2020**, *241*, 118049. [CrossRef]
39. Ishwarya, G.; Singh, B.P.; Deshwal, S.; Bhattacharyya, S. Effect of sodium carbonate/sodium silicate activator on the rheology, geopolymerization and strength of fly ash/slag geopolymer pastes. *Cem. Concr. Compos.* **2019**, *97*, 226–238.
40. Nikolov, A.; Nugteren, H.; Rostovsky, I. Optimization of geopolymers based on natural zeolite clinoptilolite by calcination and use of aluminate activators. *Constr. Build. Mater.* **2020**, *243*, 118257. [CrossRef]
41. Škvára, F.; Jílek, T.; Kopecký, L. Geopolymer materials based on fly ash. *Ceram. Silik.* **2005**, *49*, 195–204.